

Rotation Rate of Rods in Turbulent Fluid Flow

Shima Parsa,¹ Enrico Calzavarini,² Federico Toschi,³ and Greg A. Voth^{1,*}

¹*Department of Physics, Wesleyan University, Middletown, Connecticut 06459, USA*

²*Laboratoire de Mécanique de Lille CNRS/UMR 8107, Université Lille 1, 59650 Villeneuve d'Ascq, France*

³*Department of Physics, and Department of Mathematics and Computer Science, Eindhoven University of Technology, 5600 MB Eindhoven, The Netherlands*

(Received 2 May 2012; published 28 September 2012)

The rotational dynamics of anisotropic particles advected in a turbulent fluid flow are important in many industrial and natural settings. Particle rotations are controlled by small scale properties of turbulence that are nearly universal, and so provide a rich system where experiments can be directly compared with theory and simulations. Here we report the first three-dimensional experimental measurements of the orientation dynamics of rodlike particles as they are advected in a turbulent fluid flow. We also present numerical simulations that show good agreement with the experiments and allow extension to a wide range of particle shapes. Anisotropic tracer particles preferentially sample the flow since their orientations become correlated with the velocity gradient tensor. The rotation rate is heavily influenced by this preferential alignment, and the alignment depends strongly on particle shape.

DOI: [10.1103/PhysRevLett.109.134501](https://doi.org/10.1103/PhysRevLett.109.134501)

PACS numbers: 47.55.Kf, 47.27.ek, 47.27.Gs

The dynamics of anisotropic particles in turbulent fluid flows is central to understanding many applications ranging from cellulose fibers used in paper making [1] to ice crystals in clouds [2,3] to locomotion of many microorganisms [4–7]. When the particles are small and their concentration is low, their rotations are determined by the velocity gradient along their trajectories. Velocity gradients are dominated by the smallest scales in turbulence about which we have an extensive fundamental understanding [8–10]. So the statistics of rotations of anisotropic particles forms an important problem foundational to many applications for which we need to develop a predictive understanding based on the fundamental properties of turbulence.

Advances in imaging technology have made it possible to obtain time-resolved trajectories of particles in turbulence using high speed stereoscopic imaging, and these measurements have produced many new insights about Lagrangian translational dynamics of spherical particles [11]. There is also an extensive literature on the motion of anisotropic particles in fluid flows. Anisotropic particles have fascinating dynamics even in simple flows [12–15]. Several simulations have addressed the turbulent case [16–20], and experiments have measured dynamics in 2D flows [21] and orientation distributions in 3D turbulent flows [22–24]. However, there are no available experimental measurements of time-resolved rotational dynamics of anisotropic particles in 3D turbulence.

When ellipsoidal particles are small compared with the smallest length scales in the flow, their rotation rate is determined by the velocity gradient tensor through Jeffery's equation [12]:

$$\dot{p}_i = \Omega_{ij}p_j + \frac{\alpha^2 - 1}{\alpha^2 + 1}(S_{ij}p_j - p_i p_k S_{kl}p_l), \quad (1)$$

where p_i is a component of the orientation director and $\alpha \equiv l/d$, is the aspect ratio of the ellipsoid given by the ratio of length (l) to diameter (d). Ω_{ij} is the rate-of-rotation tensor, and S_{ij} is the rate-of-strain tensor which are the antisymmetric and symmetric parts of the velocity gradient tensor respectively. Particle dynamics become much more complicated when the particles are large [16] or density mismatched [2], or high particle concentration produces interparticle interactions and two-way coupling [1]. A phenomenology of the dynamics of anisotropic tracers at low concentrations in turbulence is needed to provide a foundation for continued work on the more complex cases that often appear in applications.

We have performed an experimental and computational study of rotation rates along the trajectories of anisotropic particles in turbulent flows. In the experiments, small rods are tracked using stereoscopic images from four high speed cameras. Turbulence was generated between two grids oscillating in phase in an octagonal Plexiglas tank [25] that is $1 \times 1 \times 1.5$ m³. The experiments are performed at two Taylor Reynolds numbers, $R_\lambda = (15uL/\nu)^{1/2}$, $R_\lambda = 160$ and $R_\lambda = 214$. The Kolmogorov length scale ($\eta = (\nu^3/\langle\epsilon\rangle)^{1/4}$) and time scale ($\tau_\eta = (\nu/\langle\epsilon\rangle)^{1/2}$) are $\eta = 375$ μ m and $\tau_\eta = 70$ ms at $R_\lambda = 160$, and $\eta = 210$ μ m and $\tau_\eta = 25$ ms at $R_\lambda = 214$. The rods are 1 mm in length by 200 μ m in diameter and are cut from nylon thread at a density of $\rho = 1.15$ g/cm³. These rods have length of 2.6η at $R_\lambda = 160$ and 4.8η at $R_\lambda = 214$. Reference [16] indicates that rods less than about 7η should not have a measurable change in their mean square rotation rate. The fluid is density matched with rods by adding 19% CaCl₂ by mass to water. On average there is less than one particle in the detection volume of approximately 140 cm³, so interparticle interactions are negligible. The position of the center of the rods was

measured with an uncertainty of $\approx 40 \mu\text{m}$. We have measured the orientation of rods in two dimensional (2D) images from each camera and reconstructed the orientation of rods in three dimensional (3D) space using images from multiple cameras. Determining the orientation of the rods in 3D requires measurements of the orientation in 2D images from at least three cameras that are not in the same plane. The rotation rate, $\dot{\mathbf{p}}$, is determined from quadratic fits to the measured orientation versus time data. We have also studied the motion of anisotropic tracers in direct numerical simulations (DNS) of homogeneous and isotropic turbulence at $R_\lambda = 180$. The translational motion of tracer rods matches that of fluid particles, so we are able to use a database of previously simulated Lagrangian trajectories [26] to integrate Jeffery's equation (1) and obtain the time evolution of particle orientations. The spatial spectral resolution was 512^3 points. These simulations stored the full velocity gradient tensor along Lagrangian trajectories at time intervals of about $1/10\tau_\eta$. Equation (1) has been therefore integrated *a posteriori* with the same integration time step and with an Adams-Bashforth second order in time scheme.

Figure 1 shows an experimentally measured trajectory of a 1 mm rod at $R_\lambda = 214$. This example illustrates several of the important properties of the rotation of rods. First, this rod has bursts of high rotation rate where the rotation

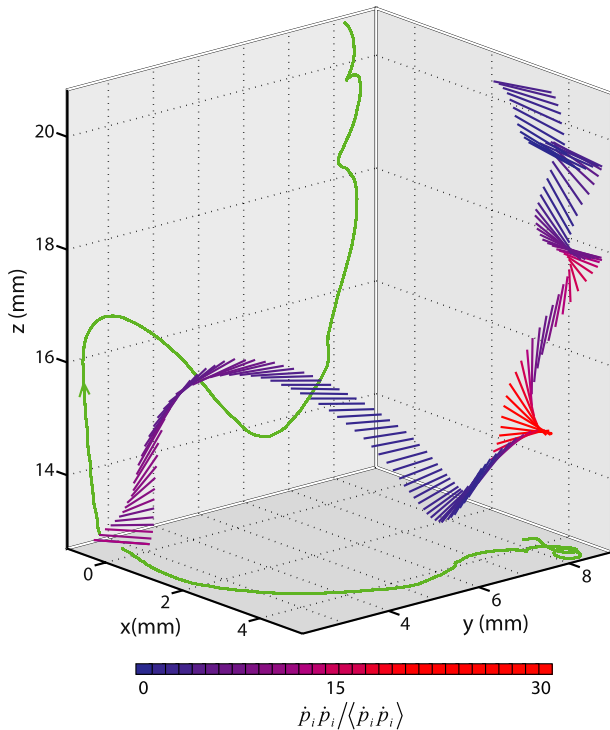


FIG. 1 (color online). Three-dimensional view of a rod trajectory with a large rotation rate from the experiment at $R_\lambda = 214$. The color of the rod represents the rotation rate. This rod is tracked for 284 ms. The green lines show the projection of the center of the rod onto the y - z and x - y planes. The rod is a circular cylinder with length 1 mm and diameter 0.2 mm.

rate squared is up to 30 times its mean, reflecting the intermittency of rod rotations. Second, in the upper right, the rod is caught in a vortex, but its rotation rate is not large because the rod has become aligned with the vorticity reflecting the tendency of anisotropic particles to become aligned by the velocity gradients in the flow.

The probability distribution function (PDF) of the rotation rate squared, $\dot{p}_i \dot{p}_i$, of rods is shown in Fig. 2(a). The PDF has long tails which indicates the presence of rare events with rotation rates squared up to 60 times the average value ($\langle \dot{p}_i \dot{p}_i \rangle$). The agreement between DNS and experiment is very good for the core of the distribution up to $20 \langle \dot{p}_i \dot{p}_i \rangle$. At larger rotation rates, the experimental

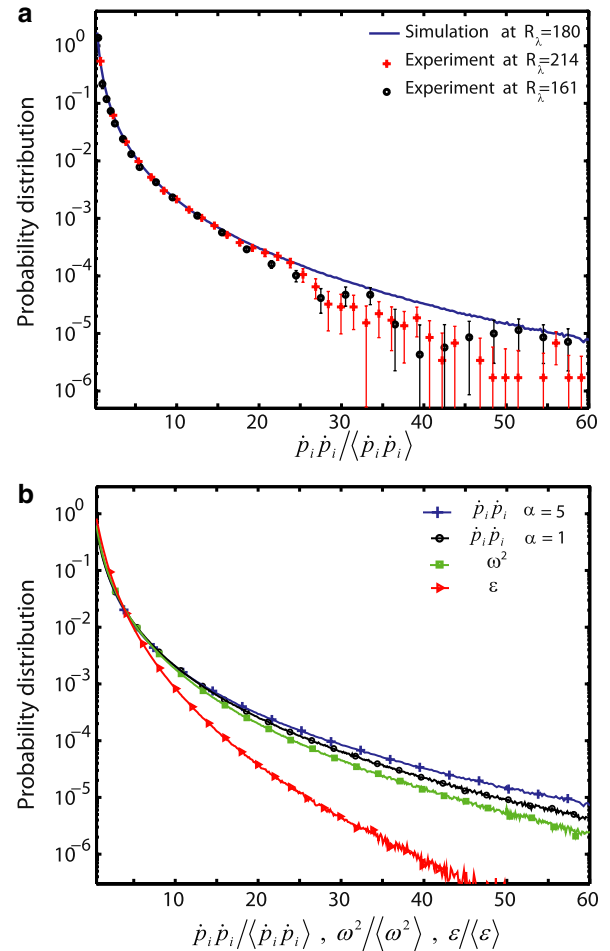


FIG. 2 (color online). The PDF of rotation rate squared of rods. (a) Comparison of simulation (blue line, $R_\lambda = 180$) with experiment (black circle, $R_\lambda = 160$; red plus, $R_\lambda = 214$) for aspect ratio $\alpha = 5$. Error bars represent both random uncertainty and the systematic uncertainty produced by measuring rotation rates from experimental orientation data over a time interval. (b) Comparison of the PDF of rotation rate squared for rods at $\alpha = 5$ (blue plus) and spheres at $\alpha = 1$ (black circle) with PDFs of enstrophy (green square) and energy dissipation rate (red triangle) for the simulation at $R_\lambda = 180$. One symbol is displayed for every twenty bins.

PDFs are slightly below the DNS. This difference is not much larger than the systematic errors in the experimental data represented by the error bars, but it may reflect the effect of the finite length of the rods in the experiment. Although Ref. [16] indicates that these should not have a measurable change from the tracer limit in their mean square rotation rate, it is possible that the rare events are more sensitive to rod length. In Fig. 2(b), the probability distribution of rotation rate squared from the numerical simulation is compared with the distributions of enstrophy ($\omega^2 = 2\Omega_{ij}\Omega_{ij}$) and energy dissipation rate ($\epsilon = 2\nu S_{ij}S_{ij}$, where ν is the kinematic viscosity). For large values of rotation rate squared, the PDF for rods ($\alpha = 5$) is larger than that of spheres ($\alpha = 1$), and both are larger than either enstrophy or energy dissipation rate. Spheres simply rotate with the vorticity, $\dot{p}_i\dot{p}_i = \Omega_{ij}\Omega_{ij}\sin^2\theta$, and the larger intermittency for spheres compared with enstrophy comes from the distribution of the angle, θ , between \mathbf{p} and the vorticity vector. Rods with $\alpha = 5$ have a contribution to their rotation rate from S_{ij} , which one might think would decrease the probability of large rotations, making it more like the distribution of the energy dissipation rate. However, variations in the orientation of the rod with respect to the velocity gradient tensor contribute additional fluctuations giving rods the most high rotation rate events.

Figure 3 shows the effect of the shape of particles on their rotation dynamics by plotting the mean square rotation rate as a function of aspect ratio, α . Our two experiments at $\alpha = 5$ are consistent with our simulations and with earlier work on thin rods at lower Reynolds numbers by Shin and Koch [16]. The simulations allow us to study the full range of aspect ratios. The mean square rotation rate of disk shaped particles ($\alpha < 1$) is much larger than that of the spheres ($\alpha = 1$). This can be qualitatively understood as the additional contribution of strain [S_{ij} in Eq. (1)] to the rotation rate. However, the rotation rate of rods ($\alpha > 1$) is much smaller than spheres even though the rate-of-strain contributes to their rotation as well.

Understanding the rotation rate data in Fig. 3 requires considering the preferential alignment that occurs between particles and the velocity gradient tensor. When particles are oriented randomly, their mean square rotation rate can be calculated analytically from Eq. (1) by extending the calculation in Ref. [16] to finite aspect ratio:

$$\frac{\langle \dot{p}_i \dot{p}_i \rangle}{\langle \epsilon \rangle / \nu} = \frac{1}{6} + \frac{1}{10} \left(\frac{\alpha^2 - 1}{\alpha^2 + 1} \right)^2. \quad (2)$$

This result is shown as the green solid curve in Fig. 3(a). As particles are advected by the flow, they become oriented so that their rotation rates are very different than the randomly oriented case, with the largest difference occurring for thin rods ($\alpha \gg 1$). Quantification of the effects of alignment with the velocity gradient tensor requires considering the alignment of the rods with the vorticity vector and the eigenvectors of the strain rate tensor. Thin tracer rods are

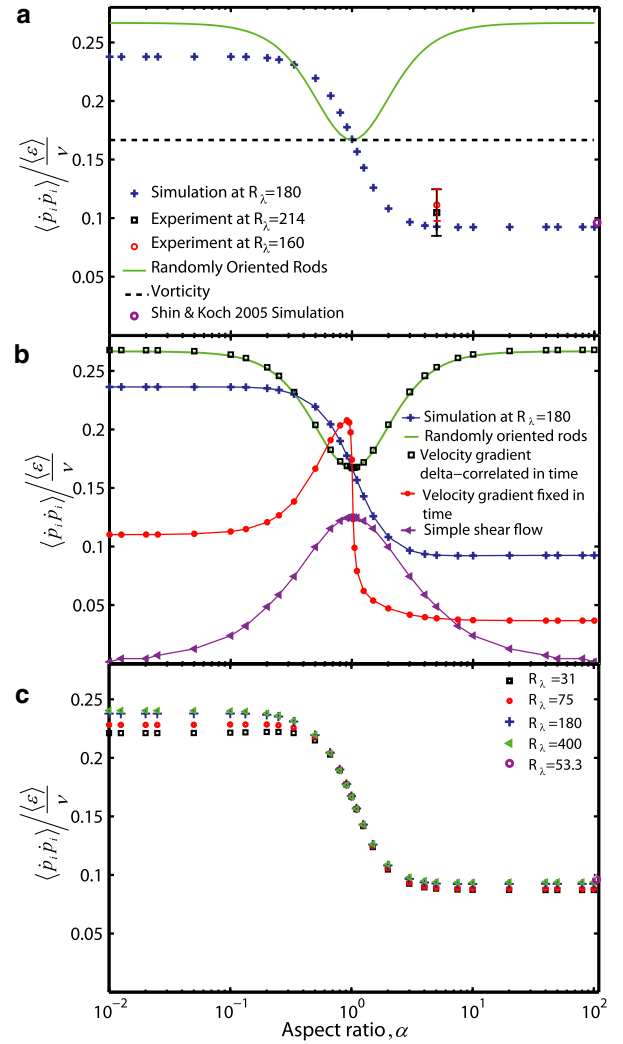


FIG. 3 (color online). Mean square rotation rate as a function of aspect ratio. (a) Blue plus is the DNS at $R_\lambda = 180$. Black open square is the experiment at $R_\lambda = 214$. Red open circle is the experiment at $R_\lambda = 160$. The error bars on the experimental points represent systematic error due to extrapolation from the finite fit time required to measure the rotation rate [29]. The purple open circle shows the result for infinite aspect ratio rods from simulations by Shin and Koch [16] at $R_\lambda = 53.3$. The green line is the analytic prediction for randomly oriented rods from Eq. (2). The dashed line indicates the rotation due to vorticity. (b) Simple cases of particles integrated through different velocity gradient fields: Blue plus uses velocity gradients along Lagrangian trajectories at $R_\lambda = 180$. Black open square uses velocity gradients sampled from the DNS and delta correlated in time. These data match the analytic prediction for randomly oriented rods shown as the green line. Red closed circle uses velocity gradients sampled from the DNS and held fixed in time. The purple right handed triangle uses the velocity gradient of a plane shear flow. (c) Comparison of simulations at different Reynolds numbers.

material line segments, and earlier work on the alignment of material lines [27,28] has shown that lines align most strongly with the vorticity and the intermediate eigenvector of the strain rate. Recent work focusing specifically on

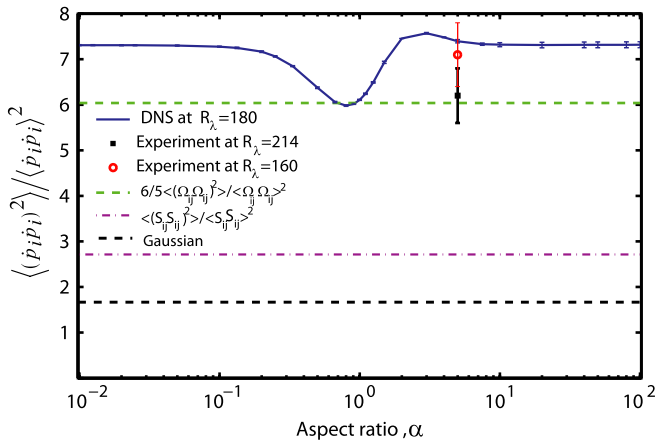


FIG. 4 (color online). Fourth moment of the rotation rate of ellipsoids. Blue plus is the DNS at $R_\lambda = 180$. Black closed square is the experiment at $R_\lambda = 214$. Red open circle is the experiment at $R_\lambda = 160$. Green dashed line is the prediction for spheres uncorrelated with the direction of Ω_{ij} . The purple dash-dotted line is the fourth moment of S_{ij} and the black dashed line represents the case of a Gaussian distribution.

tracer rods has explored the preferential alignment with vorticity in more detail [18]. Qualitatively, alignment with the vorticity will reduce the mean square rotation rate since only the vorticity perpendicular to the rod contributes to its rotation rate. However, it is not currently known how to quantitatively predict the effect of alignment on the mean square rotation rate.

Figure 3(b) shows the dependence of rotation rate on the aspect ratio for several simple cases in order to better understand the ways the data in Fig. 3(a) depend on both alignment with the velocity gradient tensor and the time evolution of the velocity gradient tensor. If the velocity gradients are sampled from DNS but are delta correlated in time, the particles do not develop alignment with the velocity gradients, and therefore the mean square rotation rate matches the prediction for randomly oriented rods in Eq. (2). When the velocity gradients are sampled from the DNS and held fixed in time, the alignment effect is too strong and the rotation rates are smaller than the rotation rates of rods advected in the turbulence at almost all aspect ratios. Finally, we integrated particles through time independent plane shear flow which generates Jeffery orbits. None of these cases has even qualitative agreement with the rotation rates of rods advected in the turbulence. Since the dependence of the mean square rotation rate on aspect ratio is sensitive to both instantaneous statistics and temporal correlations of the velocity gradient tensor, it provides a metric for evaluating models of the velocity gradient tensor in turbulence that is directly accessible experimentally.

Figure 3(c) shows the dependence of the rotation rate on the Reynolds number. In simulations ranging from $R_\lambda = 31$ to $R_\lambda = 400$, the mean square rotation rate

changes by less than 9% with the largest differences occurring for disks ($\alpha \ll 1$).

For a more quantitative evaluation of the shape of the tails of the PDF of rotation rate squared, we report in Fig. 4 a normalized fourth moment of the rotation rate, $\langle (\dot{p}_i \dot{p}_i)^2 \rangle / \langle \dot{p}_i \dot{p}_i \rangle^2$ as a function of aspect ratio. The normalized fourth moment is a measure of occurrence of extreme events. The experimental measurements are in fairly good agreement with the simulations considering that the differences are on the order of the experimental measurement errors and particle size may affect the tails of the experimental distribution as discussed above. The fourth moment for a sphere can be related to the fourth moment of the vorticity tensor by assuming that the orientation director is uncorrelated with Ω_{ij} which leads to $\langle (\dot{p}_i \dot{p}_i)^2 \rangle / \langle \dot{p}_i \dot{p}_i \rangle^2 = 6/5 \langle (\Omega_{ij} \Omega_{ij})^2 \rangle / \langle \Omega_{ij} \Omega_{ij} \rangle^2$, in good agreement with the simulations. All these fourth moments are much larger than the value of 5/3 that is obtained if the components, \dot{p}_i , have a Gaussian distribution. Rods ($\alpha \gg 1$) and disks ($\alpha \ll 1$) have nearly identical normalized fourth moments, and the variation with aspect ratio is less than 20%, indicating that the dependence on particle shape of the normalized probability distribution is much weaker than that of the mean square rotation rate in Fig. 3.

From both experiments and numerical simulations we have obtained a phenomenology of the rotational rate of ellipsoidal particles in turbulent fluid flow. Rodlike particles have a rotation rate that is strongly affected by the alignment of the rods with the vorticity vector. Disklike particles also show effects of alignment although their mean square rotation rate is closer to the randomly oriented case. The transition between the two limiting aspect ratios is quite abrupt, with 80% of the difference in mean square rotation rate between disks and rods occurring between aspect ratios 0.5 and 2. Thus for many bacteria or ice crystals that are transported in turbulent flows, the picture of a thin Lagrangian rod or disk is much better than the approximation that they are spheres.

We acknowledge support from COST Action MP0806: *Particles in turbulence* and NSF Grants No. DMR-0547712, No. DMR-1208990 and No. CNS-0959856. We thank Nicholas Ouellette for contributions to the early stages of this work.

*Corresponding author.
gvoth@wesleyan.edu

- [1] F. Lundell, D. L. Soderberg, and H. P. Alfredsson, *Annu. Rev. Fluid Mech.* **43**,195 (2011).
- [2] S. C. Sherwood, V. T. J. Phillips, and J. S. Wettlaufer, *Geophys. Res. Lett.* **33**, L05804 (2006).
- [3] M. B. Pinsky and A. P. Khain, *Atmos. Res.* **47–48**, 69 (1998).
- [4] T. J. Pedley and J. O. Kessler, *Annu. Rev. Fluid Mech.* **24**, 313 (1992).

- [5] J.D. Bowen, K.D. Stolzenbach, and S.W. Chisholm, *Limnol. Oceanogr.* **38**, 36 (1993).
- [6] D. Saintillan and M.J. Shelley, *Phys. Rev. Lett.* **99**, 058102 (2007).
- [7] J.T. Locsei and T.J. Pedley, *Bull. Math. Biol.* **71**, 1089 (2009).
- [8] B.W. Zeff, D.D. Lanterman, R. McAllister, R. Roy, E.J. Kostelich, and D.P. Lathrop, *Nature (London)* **421**, 146 (2003).
- [9] B. Luthi, A. Tsinober, and W. Kinzelbach, *J. Fluid Mech.* **528**, 87 (2005).
- [10] C. Meneveau, *Annu. Rev. Fluid Mech.* **43**, 219 (2011).
- [11] F. Toschi and E. Bodenschatz, *Annu. Rev. Fluid Mech.* **41**, 375 (2009).
- [12] G.B. Jeffery, *Proc. R. Soc. A* **102**, 161 (1922).
- [13] A.J. Szeri, W.J. Milliken, and L.G. Leal, *J. Fluid Mech.* **237**, 33 (1992).
- [14] M. Wilkinson, V. Bezuglyy, and B. Mehlig, *Phys. Fluids* **21**, 043304 (2009).
- [15] E. Gavze, M. Pinsky, and A. Khain, *J. Fluid Mech.* **690**, 51 (2011).
- [16] M. Shin and D.L. Koch, *J. Fluid Mech.* **540**, 143 (2005).
- [17] P.H. Mortensen, H.I. Andersson, J.J.J. Gillissen, and B.J. Boersma, *Int. J. Multiphase Flow* **34**, 678 (2008).
- [18] A. Pumir and M. Wilkinson, *New J. Phys.* **13**, 093030 (2011).
- [19] H.F. Zhang, G. Ahmadi, F.G. Fan, and J.B. McLaughlin, *Int. J. Multiphase Flow* **27**, 971 (2001).
- [20] C. Marchioli, M. Fantoni, and A. Soldati, *Phys. Fluids* **22**, 033301 (2010).
- [21] S. Parsa, J.S. Guasto, M. Kishore, N.T. Ouellette, J.P. Gollub, and G.A. Voth, *Phys. Fluids* **23**, 043302 (2011).
- [22] O. Bernstein and M. Shapiro, *J. Aerosol Sci.* **25**, 113 (1994).
- [23] R.K. Newsom and C.W. Bruce, *J. Aerosol Sci.* **29**, 773 (1998).
- [24] M. Parsheh, M.L. Brown, and C.K. Aidun, *J. Fluid Mech.* **545**, 245 (2005).
- [25] D.B. Blum, S.B. Kunwar, J. Johnson, and G.A. Voth, *Phys. Fluids* **22**, 015107 (2010).
- [26] R. Benzi, L. Biferale, E. Calzavarini, D. Lohse, and F. Toschi, *Phys. Rev. E* **80**, 066318 (2009).
- [27] S.S. Girimaji and S.B. Pope, *J. Fluid Mech.* **220**, 427 (1990).
- [28] M. Guala, B. Luthi, A. Liberzon, A. Tsinober, and W. Kinzelbach, *J. Fluid Mech.* **533** (2005).
- [29] G.A. Voth, A. La Porta, A.M. Crawford, J. Alexander, and E. Bodenschatz, *J. Fluid Mech.* **469**, 121 (2002).